Modeling of extrinsic defects in silica fibers using Vickers indentation

Bochien Lin
Andrew P. Stanzeski
M. John Matthewson

Fiber Optic Materials Research Program, Department of Ceramics
Rutgers University, Piscataway, NJ 08855-0909

ABSTRACT

Vickers indentation has been used to introduce controlled flaws in fused silica optical fiber in order to model the behavior of "weak" defects encountered in practice. Novel techniques are used in order to conveniently examine indentations over a broad range of residual strength; these include the use of flat fiber which facilitates specimen alignment during indentation and subsequent strength measurement in bending. The strength of indented silica fiber measured in pH 7 buffer reveals a bimodal behavior at the threshold for radial crack formation which is related to the "pop-in" of radial cracks after indentation or during strength testing. An unusually low value of the stress corrosion parameter for subthreshold indentations of $n \sim 11$ is observed in pH 7 buffer. This suggests that under some conditions the usual assumption of $n \sim 20$ may lead to an overestimation of fiber reliability.

Keywords: Vickers indentation, optical fiber, fused silica, strength, fatigue, reliability, aging.

1. INTRODUCTION

Long length optical fiber used in communications applications may be exposed to high temperatures (*e.g.* 65°C) and/or very humid environments which can severely impact their mechanical reliability.[1] Even though most of the fiber surface is pristine, during manufacturing, handling, splicing and installation, extrinsic flaws can be introduced to the fiber surface due to dust adhesion or abrasion. These kinds of defects can lead to spontaneous failure under an applied stress. Vickers indentation is commonly used to model the mechanical behavior of such flaws. For postthreshold indentations, well-defined radial cracks are observed on the fiber surface. Subthreshold indentations do not have well-defined radial cracks, but have incipient cracks within the indentation impression.[2] There exists a "threshold" region where the sub- and postthreshold behaviors overlap. In this region indentations at a given load may be either sub- or postthreshold, as seen in Fig. 1. Also, subthreshold flaws may spontaneously "pop-in" radial cracks with a substantial attendant loss of strength. Vickers indentation has the advantage of controlling the defect size, geometry and location, thus enabling analysis of the stress field around the defect.[3–6] With careful experimental techniques for indentation and strength testing, it is possible to obtain reproducible data. In this paper we describe the experimental techniques used, and in particular, the novel use of flat fiber which aids in specimen alignment. Fatigue strength data measured in pH 7 buffer and zero-stress aging results in 90°C pH 7 buffer are presented.
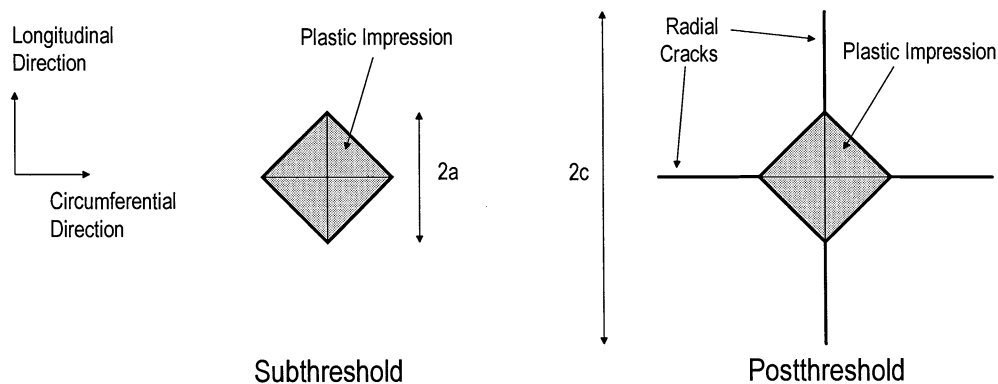

Fig. 1. Schematic of subthreshold and postthreshold indentations.

2. EXPERIMENTAL

2.1 Indentation Procedure

Bending techniques are used throughout this work in order that failure should not occur at rear surface damage introduced where the fiber is supported during indentation. No single bending technique can conveniently explore the entire strength range of interest. Therefore 2-point bending[7,8] of 100 μm diameter fiber was used to measure higher strengths while miniaturized 4-point bending[9,10] of 1000 μm diameter fiber was used for lower strengths. The two methods have a region of overlap where they yield similar results,[9] thus justifying their appropriateness. The overlap in test techniques lies well away from the threshold for radial crack formation. The strength of unindented fiber has been found independent of fiber diameter in the range of 70 μm to 1000 μm.[11]

All indentations were performed on bare fused silica fiber which had been stripped of its polymer coating by immersing in hot sulfuric acid (~200°C) for about 30 s and then rinsing with water and acetone to remove any residue. This stripping method does not affect the fiber strength.[12] A microhardness tester (equipped with a Vickers diamond pyramid indenter with a cone angle of 136°) was used with the peak indentation load maintained for 10 s, with loads ranging from 2 mN to 20N (0.2 g-f to 2 kg-f).

Given the intricacy of the techniques and the large number of specimens required to obtain statistically significant results, several approaches have been used to speed data acquisition. The bending techniques enable several fibers to be tested simultaneously. While ordinary round fiber was used early in this work, the development of flat fiber, which is fabricated by drawing from a preform whose sides have been ground flat and flame polished, as seen in Fig. 2, has several advantages. First, indentations are much easier to produce on a flat fiber since the Vickers indenter tip does not need to be accurately aligned with the apex of the curved surface of a round fiber. Furthermore, aligning the indenter tip with the fiber diameter is not necessary for flat fiber because the distance from the neutral axis during bending is the same across the flat. Lastly, when bent, the fiber automatically bends in the direction of minimum second moment of area, *i.e.*, the neutral axis is always parallel to the flats on the fiber. The indentation therefore automatically aligns on the surface of maximum tension. This obviates the need for careful azimuthal alignment of the indentation. However, there is a possibility that the residual stress field of an indent on a flat fiber will be different from that on a cylindrical fiber due to the difference in geometry. However, both specimen geometries have been found to give similar strength and fatigue results.
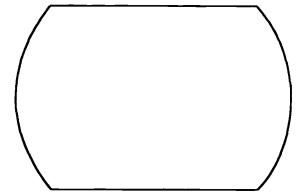

Fig. 2. Cross-section of the flat fiber geometry.

A length of fiber was broken into 1000 specimens. Samples for any given experiment were then selected randomly from this batch in order to avoid any influence from systematic variations along the fiber length. After stripping, each specimen was indented on the flat surface between two dots made with a permanent marker. The indentation diagonal, 2*a*, and radial crack length, 2*c*, (if present) were measured. The marker dots are used to identify the location of the indent during subsequent testing. For longer aging times an additional high load indent was applied at one end of the fiber to act as a marker for easy identification of the side of the fiber containing the indent of interest. This was necessary since the marker dots sometimes washed off after prolonged aging in 90°C pH 7 buffer. Fibers were protected from contacting each other during aging by placing in a holder that keeps them separate. After aging, each fiber was rinsed with water and acetone to clean the surface and then re-examined under an optical microscope to observe if radial cracks had "popped in" during aging. The fiber was then broken in either a 2- or 4-point bend apparatus with the indent on the tensile side of the bend. Finally, the two fragments had their fracture surfaces evaluated and then preserved for future reference.

2.2 Strength Measurement Procedure

The 2-point bending technique[7,8] used for the stronger indents (*i.e.* lower indentation loads), has the fiber bent 180° and held between two faceplates, which are brought together by a computer-controlled stepper motor until the fiber breaks. The break is detected acoustically and the faceplate separation, *d,* is recorded. The failure strain, ε_f, is calculated by:

$$\varepsilon_f = \frac{1.198 \, d_f}{d + d_g - d_f} \, ,$$ (1)

where d_f is the fiber diameter and d_g is the depth of the groove. The apparatus was used in constant strain rate mode which requires the faceplate velocity, $\dot{d}$, to vary continuously with the separation, d.[13,14] The fiber was carefully aligned between the faceplates so that the indent lay on the tip of the bend on the tensile surface to be sure that the indent experienced the maximum strain given by Eq. 1. The problems of fiber rotation and twisting can be solved more easily by using flat fiber instead of cylindrical fiber.

For "weaker" indents the failure strain was measured using a 4-point bending apparatus with load at the quarter points.[9,10] The fiber is threaded between 4 pins, of which the inner two push the fiber against the two outer pins until failure occurs. The failure strain, ε_f, is calculated by:[9]

$$\varepsilon_f = \frac{3 d_f D}{2 a^2} \, ,$$ (2)

where D is the travel distance of the center pins and $4a$ is the outer pin separation. This technique has several significant advantages. Arbitrarily weak fiber can be tested since it is loaded into the apparatus under zero stress. Also, several fibers can be tested simultaneously, and the "single ended" pin design permits the specimens to be easily immersed in liquid test environments.

The dynamic fatigue behavior of the indents was characterized by measuring the failure strain, ε_f, as a function of strain rate, $\dot{\varepsilon}$. The apparent stress corrosion susceptibility parameter, n, was then calculated from the slope of a $\log\varepsilon_f$ vs. $\log\dot{\varepsilon}$ plot, namely:

$$\frac{1}{n+1} = \frac{d \log \varepsilon_f}{d \log \dot{\varepsilon}} \, .$$ (3)

The apparent n-value for each load was calculated based on four strain rates spanning three decades. In general, n is not the true susceptibility parameter, n_0, which is defined by crack velocity measurements. The two values are very different for indentations due to the influence of the residual stresses associated with the indent.

3. RESULTS & DISCUSSION

Fig. 3 shows the strain to failure, ε_f, measured in room temperature pH 7 buffer solution at a strain rate of 10 %·min^{-1}, as a function of indentation load, P. The fibers were indented and then immediately tested. It is noted that, though there is no overlap, the 2- and 4-point data are collinear in the subthreshold region and thus give compatible results. The slope in Fig. 3 is -0.326 ± 0.007 for the subthreshold region and -0.236 ± 0.07 in the postthreshold region. The bimodal strength behavior seen in Fig. 3 for 2 N indentations is caused by the stochastic nature of the radial cracks. The low strength mode corresponds to indents with radial cracks, while indents without radial cracks lead to the high strength mode.

The threshold for radial crack formation, i.e. "pop-in," occurs over a range of loads which depends somewhat on the surrounding environment and the length of time after indenting. For short times after indenting, such as a few seconds in air, 3 N indents typically pop-in. For much longer aging times, such as 1 week in 90°C pH 7 buffer, many, but not all, 0.25 N indents pop-in. An optical microscope was used to determine whether radial cracks had popped-in before testing. Fractography was used to determine if indents popped-in during testing; the fracture surface showed crack arrest lines for radial cracks which popped-in stably before final catastrophic failure. Lateral cracks are readily observed for indentation loads greater than 10 N without aging. After prolonged aging of the indents in 90°C pH 7 buffer, lateral cracks were seen in loads as low as 0.5 N. Also, shallow corner and edge cracks were found for 0.1 to 0.25 N indents while shallow ring cracks were observed for 0.5 N indents. The relation of corner, edge and ring crack "pop-in" to strength reduction of subthreshold flaws has not been reported in the literature.
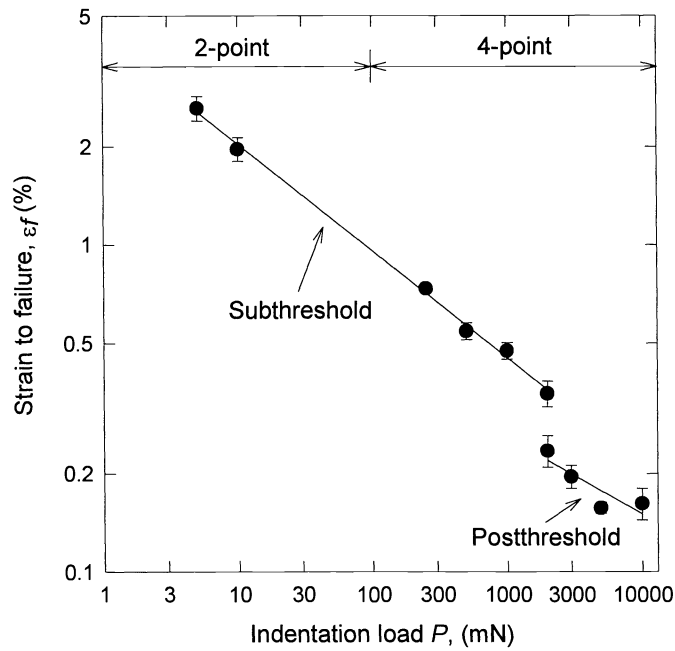
Fig. 3. Strain to failure, ε_f, as a function of indentation load, P, for silica fiber tested in $22\pm2°C$ pH 7 buffer at a strain rate of 10 %·min⁻¹.
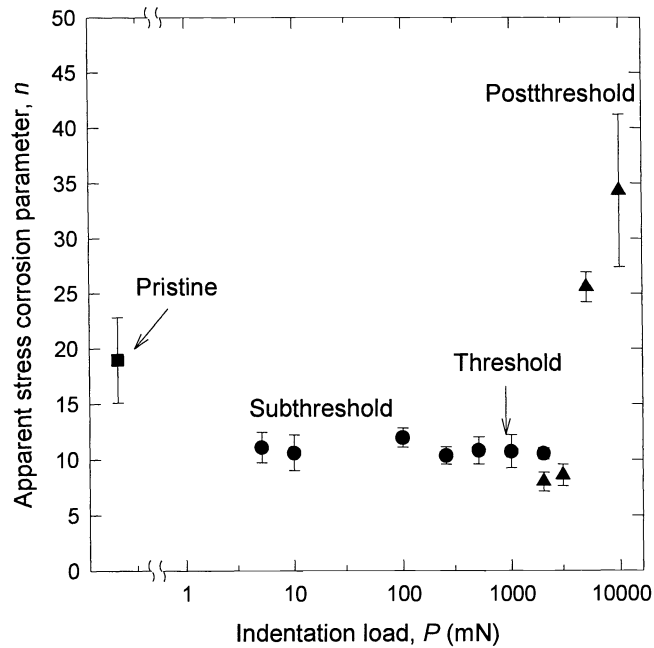

Fig. 4. Apparent stress corrosion parameter, n, as a function of the indentation load, P, for the silica fiber tested in pH 7 buffer solution at $22\pm2°C$.
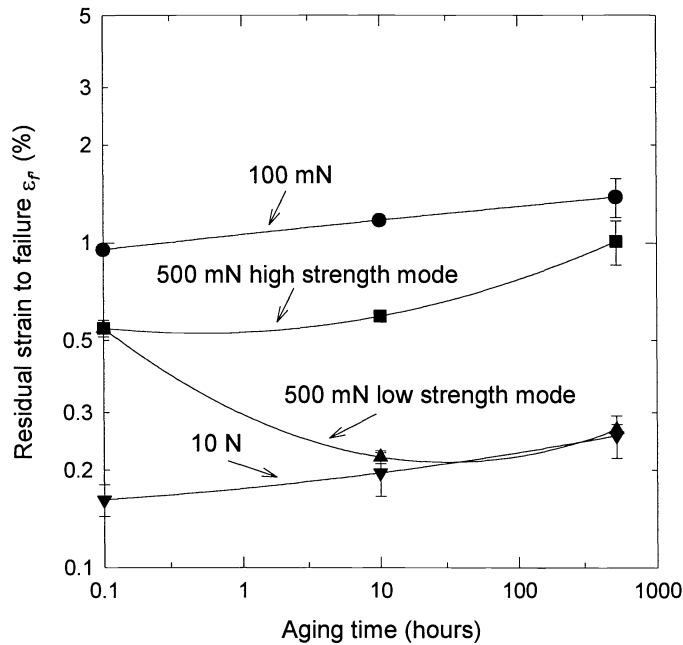
Fig. 5. Residual strength of 0.1, 0.5 and 10 N indents measured in room temperature pH 7 buffer as a function of zero stress aging time in 90°C pH 7 buffer.

Fig. 4 shows the apparent stress corrosion parameter, n, as a function of the indentation load, P, for the silica fiber tested in room temperature pH 7 buffer. It is seen that the n-value is independent of indentation load in both the sub- and postthreshold regions, with $n \sim 11$ in the subthreshold and $n \sim 30$ in the postthreshold region. At the threshold for unaged fiber, which is between 2 to 3 N, bimodal behavior is expected. However, most 2 and 3 N indents which had not "popped-in" after indenting had "popped-in" during testing and therefore, a good statistical determination of n for the high strength mode at these loads is yet to be made. The subthreshold behavior shows no tendency for n to increase at low loads towards a value of 20, characteristic of pristine fiber. However, it was observed to be about 20 for subthreshold indents measured in air.[4]

Fig. 5 shows the residual strength as a function of zero stress aging time in 90°C pH 7 buffer for indentations made at three different loads. The strength for the subthreshold (100 mN, far from the threshold) and postthreshold (10 N) indentations increases monotonically with aging time, which is in agreement with the results of Glaesemann[15] for the aging behavior of abraded fiber. However, bimodal behavior is observed for the 0.5 N subthreshold indents. After 10 hours of zero-stress aging a low strength mode appears which is the result of radial crack pop-in during aging or the subsequent strength test. An optical microscope was used to verify if pop-in occurred during aging while fractography was used to verify if radial cracks popped-in during strength testing. It is noted that the radial crack pop-in behavior for the near-threshold flaws after prolonged aging times endangers the validity of fiber lifetime estimations since the abrupt loss of strength associated with pop-in is not considered in current reliability prediction models which only consider the behavior of simple residual stress-free cracks.

Cook and Lawn[16] modeled the postthreshold radial crack as an ideal center-loaded penny shaped surface crack and incorporated the residual stress field using Hill's classical expanding elastic-plastic cavity model, as well as the applied stress field. They derived a relationship between the dynamic fatigue strength, σ_f, and the indentation load, P, as:

$$\log \sigma_f + \frac{1}{3} \log P = \frac{1}{(n_0 + 1)} \left[\log P + \log(\lambda'_p \dot{\sigma}_a) \right] , \tag{4}$$

where λ'_p is an intercept term independent of the load P, $\dot{\sigma}_a$ is the applied stress rate and n_0 is the true stress corrosion coefficient. In the presence of residual stress, the apparent stress corrosion susceptibility parameter for the indentation, n, determined by dynamic fatigue measurements is given by:[16]

$$n = \frac{3}{4} n_0 + \frac{1}{2} . \tag{5}$$

If the crack were residual stress free, then $n = n_0$. For $n_0 \gg 1$, the slope of $\log \sigma_f$ vs. $\log P$ plot is $-1/3$. Lathabai et al.[17] predicted a slope of $-1/4$ for the $\log \sigma_f$ vs. $\log P$ plot in their model for subthreshold flaws. Using classical penny shaped crack mechanics with due consideration of near field residual stress as a driving force for crack initiation, Choi et al.[6] proposed an approximate derivation for the inert strength, σ_p, for subthreshold flaws in the propagation controlled regime:

$$\sigma_p = \left[\frac{0.47 K_c^{4/3}}{(\Gamma + \Phi)^{1/3} \Psi \, a^{2/3}} \right] , \tag{6}$$

where Γ, Ψ and Φ are empirical load independent constants related to the near-field and far-field residual stresses, and the applied stress field, respectively. Using the definition of hardness, $H = P/2a^2$, a slope of $-1/3$ is derived from the subthreshold $\log \sigma_f$ vs. $\log P$ plot, since the stress intensity factor, K_c, is load independent.

Inserting the postthreshold n-value of 30 into Eq. 4, the predicted slope of $-1/3 + 1/(n_0+1)$ is ~ -0.292. A large gap exists between this value and our postthreshold data with a slope of -0.236 ± 0.07 indicating that the Cook and Lawn dynamic fatigue model[16] and the Lathabai's, et al. subthreshold model[17] can not correctly predict the n-value behavior near the threshold. Another possibility is the assumption of $\sigma \cdot P^{1/3} =$ constant is not valid near the threshold since our postthreshold measurement is limited to a range of 3 to 10 N indentations, which is a short span for the postthreshold regime. However, the subthreshold model for the propagation controlled strength, developed by Choi et al.[6] predicts a $-1/3$ slope that fits our data in pH 7 buffer as well as air.[18] There is still no single model that can completely predict the slope behavior of both the sub- and postthreshold flaws.

A model for postthreshold flaws by Dabbs and Lawn[4] predicted that the residual stress field reduces the n-value to $n \sim 30$, from the true value of $n_0 \sim 40$. They suggested that a bigger reduction for subthreshold flaws explains the value of $n \sim 19$ in air. Also, Choi et al.[6] found $n \sim 14$ for subthreshold indentations tested in air. Gulati[19] asserts that strengths of fibers with large flaws increase after zero-stress aging and therefore, the deterioration of strength from a small flaw does not impair service reliability and, hence, should not be of concern to the end users because the fiber strength is controlled by the largest flaw on the fiber surface whose properties *improve* with time. However, these arguments ignore the possibility of both pop-in and abnormally low n-values as we observe for subthreshold indents in pH 7 buffer.

4. CONCLUSIONS

We have studied sub- and post-threshold indentations on fused silica optical fiber, and characterized their strength and aging behavior in pH 7 buffer. We suggest indents model the kind of behavior that might be exhibited by "real" defects, some of which also have intense residual stress fields. If this is accepted, the results have serious implications for fiber reliability. Currently, reliability models make predictions with the assumption of a sharp, stress-free crack. The behavior of indents shows substantial deviations from the simple crack model which therefore is not appropriate even if it is assumed the crack has properties such as effective length and effective fatigue parameter. In particular, the apparent n-value is very sensitive to environment with a value ~ 10 in pH 7 buffer and ~ 20 in air for subthreshold indentations. Generally, aging of indents agrees with observations in other work on weak fiber in that the strength and n increase with aging time. However, the important exception is in the

threshold region where the strength of indents decreases with aging; the threshold region is important since it is in the range of typical proof stresses. Clearly, further understanding is required before we can make rational reliability predictions.

5. ACKNOWLEDGMENTS

6. REFERENCES

1. S. V. Lisle and T. C. Tweedie, "Fiber and cable reliability," *Lightwave*, November, 38-39 1993.
2. B. R. Lawn, T. P. Dabbs and C. J. Fairbanks, "Kinetics of shear-activated indentation crack initiation in soda-line glass," *J. Mat. Sci.*, **18** 2785-2797 1983.
3. B. R. Lawn, K. Jakus and A. C. Gonzalez, "Sharp vs blunt crack hypothesis in the strength of glass: a critical study using indentation flaws," *J. Am. Ceram. Soc.*, **68** 25-34 1985.
4. T. P. Dabbs and B. R. Lawn, "Strength and fatigue properties of optical glass fibers containing microindentation flaws," *J. Am. Ceram. Soc.*, **68** [11] 563-569 1985.
5. R. F. Cook and G. M. Pharr, "Direct observation and analysis of indentation cracking in glasses and ceramics," *J. Am. Ceram. Soc.*, **73** [4] 787-817 1990.
6. S. R. Choi, J. E. Ritter, Jr. and K. Jakus, "Failure of glass with subthreshold flaws," *J. Am. Ceram. Soc.*, **73** [2] 268-274 1990.
7. P. W. France, M. J. Paradine, M. H. Reeve and G. R. Newns, "Liquid nitrogen strengths of coated optical glass fibres," *J. Mat. Sci.*, **15** 825-830 1980.
8. M. J. Matthewson, C. R. Kurkjian and S. T. Gulati, "Strength measurement of optical fibers by bending," *J. Am. Ceram. Soc.*, **69** [11] 815-821 1986.
9. G. J. Nelson, M. J. Matthewson and B. Lin, "A novel four-point bend test for strength measurement of optical fibers and thin beams: Part I: bending analysis," *J. Lightwave Tech.* in press.
10. M. J. Matthewson and G. J. Nelson, "A novel four-point bend test for strength measurement of optical fibers and thin beams: Part II: statistical analysis," *J. Lightwave Tech.* in press.
11. B. Lin, M. J. Matthewson and C. R. Kurkjian, "The diameter dependence of the strength of fused silica fibers," unpublished work.
12. M. J. Matthewson, C. R. Kurkjian and J. R. Hamblin, "Acid stripping of fused silica optical fibers without strength degradation," submitted to *J. Lightwave Tech.*.
13. H. H. Yuce, M. E. Melczer and P. L. Key, "Mechanical properties of optical fibers in bending," *IOOC '89 Tech. Digest*, **2** 44-55 1989.
14. V. V. Rondinella and M. J. Matthewson, "Effect of loading mode and coating on dynamic fatigue of optical fiber in two-point bending," *J. Am. Ceram. Soc.*, **76** [1] 139-144 1993.
15. G. S. Glaesemann, "The mechanical reliability of large flaws in optical fiber and their role in reliability predictions," *Proc. 41st Int. Wire & Cable Symp.*, 698-704 1992.
16. R. F. Cook and B. R. Lawn, "Controlled indentation flaws for construction of toughness and fatigue master maps" in "Methods for assessing the structural reliability of brittle materials," eds. S.W. Freiman and C.M. Hudson, 22-42 ASTM, Philadelphia, 1984.
17. S. Lathabai, J. Rödel, T. P. Dabbs and B. R. Lawn, "Fracture mechanics model for subthreshold indentation flaws: Part I equilibrium fracture," *J. Mat. Sci.*, **26** 2157-2168 1991.
18. B. Lin, M. J. Matthewson and G. J. Nelson, "Indentation experiments on silica optical fibers," *Proc. Soc. Photo-Opt. Instrum. Eng.*, **1366** 157-166 1990.
19. S. T. Gulati, "Large flaws: the culprit in fiber reliability," *Photonics Spectra*, **26** [12] 78-82 1992.